DYNAMICS OF THE SOLAR MAGNETIC NETWORK: TWO-DIMENSIONAL MHD SIMULATIONS

S. S. HASAN

Indian Institute of Astrophysics, Bangalore 560034, India; hasan@iiap.res.in

A. A. VAN BALLEGOOIJEN AND W. KALKOFEN

Harvard-Smithsonian Center for Astrophysics, 60 Garden Street, Cambridge, MA 02138

AND

O. STEINER

Kiepenheuer-Institut für Sonnenphysik, 7800 Freiburg, Germany

ABSTRACT

The aim of this work is to identify the physical processes that occur in the network and contribute to its dynamics and heating. We model the network as consisting of individual flux tubes, each with a nonpotential field structure, that are located in intergranular lanes. With a typical horizontal size of about 150 km at the base of the photosphere, they expand upward and merge with their neighbors at a height of about 600 km. Above a height of approximately 1000 km the magnetic field starts to become uniform. Waves are excited in this medium by means of motions at the lower boundary. We focus on transverse driving, which generates both fast and slow waves within a flux tube and acoustic waves at the interface of the tube and the ambient medium. The acoustic waves at the interface are due to compression of the gas on one side of the flux tube and expansion on the other. These longitudinal waves are guided upward along field lines at the two sides of the flux tube, and their amplitude increases with height due to the density stratification. Being acoustic in nature, they produce a compression and significant shock heating of the plasma in the chromospheric part of the flux tube. For impulsive excitation with a time constant of 120 s, we find that a dominant feature of our simulations is the creation of vortical motions that propagate upward. We have identified an efficient mechanism for the generation of acoustic waves at the tube edge, which is a consequence of the sharp interface of the flux concentration. We examine some broad implications of our results.

Subject headings: MHD — Sun: chromosphere — Sun: magnetic fields — Sun: oscillations

Online material: color figure

1. INTRODUCTION

The quiet solar chromosphere is bifurcated into the magnetic network on the boundary of supergranulation cells and the largely field-free internetwork medium in the cell interior, with respective filling factors in a 2:3 ratio in the middle chromosphere (i.e., at a height of about 1 Mm above the level of unit optical depth at 5000 Å). The network is about 30% brighter in Ca II K_{2v} emission than the internetwork chromosphere (Skumanich et al. 1975). Both the network and the internetwork media show bright points (BPs), which are prominent in the emission peaks in the cores of the Ca II H and K lines, formed in the middle chromosphere. However, the dynamical and spectral properties of network and internetwork BPs are quite different. In internetwork areas the chromospheric velocity power spectrum is dominated by oscillations with frequencies at and above the acoustic cutoff frequency (period of 3 minutes in upper photosphere; e.g., Rutten & Uitenbroek 1991), whereas in the network, Ca II H line-center velocity and intensity power spectra are dominated by low-frequency oscillations with periods of 7–20 minutes (Lites et al. 1993). These long-period waves have also been observed at larger heights (Curdt & Heinzel 1998; McAteer et al. 2002, 2003). Furthermore, network BPs show high emission in the line core most of the time (Lites et al. 1993), whereas internetwork locations have a bright phase only about 5%–10% of the time (von Uexküll & Kneer 1995). Finally, 80% of network BPs have symmetric profiles in the line core, with more or less equal intensity in the blue and red emission peaks on either side of the central absorption. In contrast, only about 30% of internetwork BPs have symmetric profiles, and 40% have blue-peak enhancements (Grossmann-Doerth et al. 1974), hence the name H_{2v} or K_{2v} bright point.

While the qualitative properties of internetwork BPs are reasonably well understood, including their formation in upward-propagating acoustic shocks that encounter downward-flowing gas (Carlsson & Stein 1995), this is not true for network BPs. The physical processes that heat the magnetic network have not been fully identified. Are network BPs heated by wave dissipation, and if so, what is the nature of these waves? How can we understand the observed relatively constant emission and symmetric line profiles of network BPs? The source of energy for network BPs is likely to be magnetohydrodynamic waves. Possible candidates are

1. kink (transverse) waves, generated inside flux tubes by the buffeting action of granules,

2. longitudinal waves, generated by pressure fluctuations inside flux tubes,

3. torsional (Alfvén) waves, generated inside flux tubes,

4. acoustic waves generated in the field-free atmosphere surrounding flux tubes, that penetrate into the tubes, and

5. acoustic waves generated at the interface of flux tubes and the outside medium, that also penetrate into flux tubes.

The first three are well-known flux tube modes (e.g., Spruit 1981). Several investigations have focused on the generation and propagation of transverse and longitudinal wave modes and their dissipation in the chromosphere (e.g., Zhugzhda et al. 1995; Fawzy et al. 2002; Ulmschneider 2003 and references therein). Torsional waves have received some attention (e.g., Hollweg

et al. 1982; Noble et al. 2003). The fourth wave type is an obvious source since it is responsible for heating the internetwork medium. However, the importance of the fifth wave type, which we found during the course of this investigation, does not appear to have been adequately recognized earlier. It will be discussed in more detail later on.

The present study is a continuation of earlier work on the excitation of transverse and longitudinal waves in magnetic flux tubes by the impact of fast granules on flux tubes (Hasan & Kalkofen 1999), as observed by Muller & Roudier (1992) and Muller et al. (1994), and following the investigation by Choudhuri et al. (1993), who studied the generation of kink waves by footpoint motion of flux tubes. The observational signature of the modeled process was highly intermittent in radiation emerging in the H and K lines, contrary to observations. When we added waves that were generated by high-frequency motion due to the turbulence of the medium surrounding flux tubes (Hasan et al. 2000), the energy injection into the gas inside a flux tube became less intermittent, and the time variation of the emergent radiation was in better agreement with the more steady observed intensity from the magnetic network.

The above studies modeled wave excitation and propagation in terms of the Klein-Gordon equation, motivated by the identification of the power peak near 7 minutes in the observed power spectrum (Lites et al. 1993; Curdt & Heinzel 1998; McAteer et al. 2002) with the cutoff period of kink waves in thin magnetic flux tubes (Kalkofen 1997). This analysis was based on a linear approximation in which the longitudinal and transverse waves are decoupled. However, it is well known that the velocity amplitude $v(z)$ for the two modes increases with height z [for an isothermal atmosphere, as $v \propto \exp(z/4H)$, where H is the pressure scale height], so that the motions are expected to become supersonic higher up in the atmosphere. At such heights, nonlinear effects become important, leading to a coupling between the transverse and longitudinal modes. Some progress on this question has been made in one dimension, using the nonlinear equations for a thin flux tube, by Ulmschneider et al. (1991), Huang et al. (1995), and Zhugzhda et al. (1995), and more recently by Hasan et al. (2003) and Hasan & Ulmschneider (2004), who examined mode coupling between transverse and longitudinal modes in the magnetic network. By solving the nonlinear, time-dependent MHD equations, they found that significant longitudinal wave generation occurs in the photosphere, typically for Mach numbers as low as 0.2, and that the onset of shock formation occurs at heights of about 600 km above the photospheric base, accompanied by heating (Hasan et al. 2003; Hasan & Ulmschneider 2004). The efficiency of mode coupling was found to depend on the magnetic field strength in the network and is a maximum for field strengths corresponding to $\beta \approx 0.2$, when the kink and tube wave speeds are almost identical. This can have interesting observational implications. Furthermore, even when the two speeds are different, once shock formation occurs, the longitudinal and transverse shocks exhibit strong mode coupling.

The above studies on the magnetic network make use of two important idealizations: they assume that the magnetic flux tubes are thin, an approximation that becomes invalid at about the height of formation of the emission peaks in the cores of the H and K lines, and they neglect the interaction of neighboring flux tubes. Some progress in this direction has recently been made by Rosenthal et al. (2002) and Bogdan et al. (2003), who studied wave propagation in a two-dimensional stratified atmosphere, assuming a potential magnetic field to model the network and internetwork regions on the Sun. They examined the propagation of waves that are excited from a spatially localized source in the photosphere. Their results indicate that there is strong mode coupling between fast and slow waves at the so-called magnetic canopy, which they identify with regions where the magnetic and gas pressures are comparable. As a consequence of the potential-field approximation, some magnetic field lines are nearly horizontal even at the base of the field. Such a model may not be appropriate for a network patch, which is perhaps better idealized as a collection of vertical tubes (Cranmer & van Ballegooijen 2005).

Thus, the problem that we address concerns wave propagation in regions that are largely representative of individual structures in the magnetic network—this is different from the one analyzed by Rosenthal et al. (2002) and Bogdan et al. (2003). Our initial configuration consists of flux tubes in two-dimensional magnetostatic equilibrium with a sharp interface between the tube and the surrounding gas. Waves are generated in this medium by means of transverse motion at the lower boundary, which displaces the entire flux tube, unlike the problem studied in the above papers, in which the source region is confined to a portion of the magnetic structure. This can have interesting consequences, some of which were unrecognized thus far. These are explored below. Our calculations indicate the presence of a new and efficient mechanism for longitudinal wave generation and shock formation in the chromosphere.

The present study forms the first of a series devoted to a detailed investigation of wave propagation in the magnetic network. As a first step, we go beyond the thin flux tube approximation and employ a two-dimensional treatment in slab geometry, similar to Rosenthal et al. and Bogdan et al. For simplicity, we neglect nonadiabatic effects at this stage, which we will include in a separate paper.

Several papers have looked at MHD waves in various geometries in the solar atmosphere using multidimensional simulations (e.g., Shibata 1983; Cargill et al. 1997; Ofman & Davila 1998; Sakai et al. 1998; Ofman et al. 1999; additional references can be found in Bogdan et al. 2003).

The organization of this paper is as follows: in § 2 we describe the initial equilibrium model, its construction and in § 3 the numerical method of solution along with the driving mechanism. The results of our calculation are presented in § 4, followed by a discussion and summary in § 5.

2. MODEL

Following Cranmer & van Ballegooijen (2005), we treat a network element (typical flux $\sim 3 \times 10^{19}$ Mx) as consisting of a collection of smaller flux tubes that are spatially separated from one another in the photosphere. The gas pressure in the atmosphere decreases with increasing height, causing a lateral expansion of the flux tubes. Neighboring flux tubes within the network element merge into a monolithic structure at some height. Above this "merging height" the network element consists of a single thick flux tube that further expands with height. The outer edge of this tube forms a magnetic canopy that overlies the neighboring supergranular cells. A second merging occurs when neighboring network elements come together at a canopy height. Figure 1 schematically shows the picture we have for the network field structure. It consists of three distinct regions:

1. *Photospheric region up to about* 0.6 Mm.—Consisting of individual flux tubes, this region has a typical diameter of 200 km in the low photosphere. Their footpoints are located in intergranular lanes and separated from one another by about the diameter of a granule (~ 1 Mm). They expand upward and merge with their neighbors at a height of about 0.6 Mm.
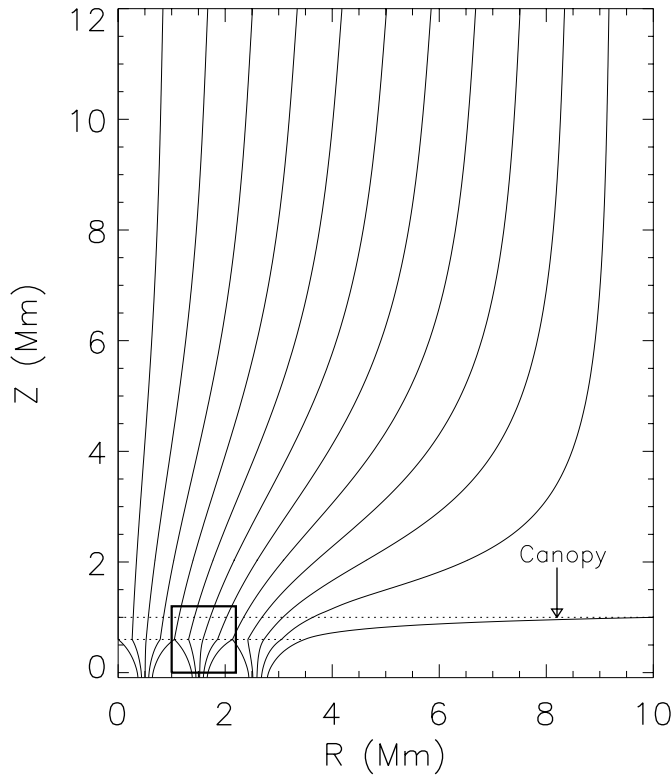
Fig. 1.—Model of a network element consisting of individual flux tubes separated at the photospheric surface by a distance of 1000 km that merge at a height of about 600 km. The box corresponds to the domain taken up for dynamical simulations. [*See the electronic edition of the Journal for a color version of this figure.*]

2. *Lower chromosphere, between the heights of* 0.6 *and* 1 Mm.—The merged network flux element expands laterally over the surrounding supergranular cell center and overlying field-free chromosphere.

3. *Upper chromosphere and corona, between* 1 *and* 12 Mm.— The fully merged magnetic field fills the available volume. At larger heights, the field expands primarily in the vertical direction and becomes more or less uniform. However, at lower heights, between 1 and 2 Mm, the field strength varies significantly with horizontal position, and the field strength directly above the flux tubes (Fig. 1, *left*) is much larger than above the supergranular cell center (Fig. 1, *right*).

Our model is based on the idea that the base of flux tubes is located in subsurface layers, where convective flows may be different from those in the visible photosphere. Flux tubes occur in regions with convective downflows below intergranular lanes. These downflows are likely to be highly turbulent, involving lateral motions that produce transverse waves in the flux tubes. When the upward-propagating waves reach the photosphere, they cause horizontal motions of flux tubes relative to their local surroundings. This generates excess pressure on the leading edge of a flux tube and a pressure deficit on the trailing edge. Our two-dimensional MHD calculations (see § 3) indicate that these pressure pulses produce an upward-velocity pulse on the leading side of the flux tube and a downward pulse on the trailing side. These pressure pulses and vertical flows are an integral part of the MHD wave, so the transverse and longitudinal motions are strongly coupled.

2.1. *Initial Two-dimensional Magnetostatic Model*

Let us consider an individual flux tube at the base of a magnetic network element on the quiet Sun; the region of interest is

indicated by the small box in Figure 1. At heights below about 600 km, the flux tubes are spatially distinct from one another and are embedded in a field-free "external" medium. At $\approx$1000 km, the flux tubes merge into a more uniform field. The structure of the flux tube at the initial instant is assumed to be in static equilibrium and is determined by the magnetostatic force balance equation:

$$-\nabla p + \rho \boldsymbol{g} + \frac{1}{4\pi}(\nabla \times \boldsymbol{B}) \times \boldsymbol{B} = 0, \qquad (1)$$

where $\boldsymbol{g} = -g\hat{\boldsymbol{z}}$ is the gravitational acceleration, p is the gas pressure, ρ is the density, and $\boldsymbol{B}$ is the magnetic field. The third term in equation (1) describes the Lorentz force due to electric currents at the boundary between the flux tube and its local surroundings.

We have developed a numerical code for solving equation (1) in two dimensions; all quantities are assumed to be independent of the horizontal y-coordinate, so the flux tubes are approximated by sheets. However, despite this difference we continue to use the term flux tube to represent a flux sheet. We consider a rectangular domain $x = [L, 2L]$ and $z = [0, H]$, representing one-half of a flux sheet; $x = L$ is the flux sheet axis, $x = 2L$ is the interface with the neighboring sheet on the right, and $z = 0$ is the base of the photosphere. The magnetic field is written in terms of a flux function $A(x, z)$:

$$B_x = -\frac{\partial A}{\partial z}, \qquad B_z = \frac{\partial A}{\partial x}. \qquad (2)$$

The distribution of $A(x, 0)$ at the lower boundary is computed from the pressure balance condition for a thin flux sheet: $p + B_z^2/8\pi = $ constant along the bottom boundary. The boundary conditions for A are $A(L, z) = 0$ and $A(2L, z) = A_{\max}$, where $A_{\max}$ is one-half of the total magnetic flux within the sheet. The gas pressure and density are expressed as

$$p = p_{\text{int}}(z)\big[1 + \beta_0^{-1}F(A)\big], \qquad (3)$$

$$\rho = \rho_{\text{int}}(z)\big[1 + \beta_0^{-1}F(A)\big], \qquad (4)$$

respectively, where $p_{\text{int}}(z)$ is the internal gas pressure as function of height along the axis of the flux sheet, $\rho_{\text{int}}(z)$ is the internal density, $\rho_{\text{int}}(z) = -g^{-1}dp_{\text{int}}/dz$, β_0 is the ratio of gas and magnetic pressures at the base (on axis), and $F(A)$ is a function describing the variation of gas pressure across field lines. Note that the temperature depends only on height (p/ρ is independent of x). The function $F(A)$ varies from zero on the axis of the sheet to $F(A_{\max}) = 1$ in the external medium, resulting in distributed electric currents at the interface between the sheet and its local surroundings.

Inserting equations (2), (3), and (4) into equation (1) yields

$$\nabla^2 A + 4\pi p_{\text{int}}(z)\beta_0^{-1}\frac{dF}{dA} = 0, \qquad (5)$$

which can be solved by minimizing the following Lagrangian:

$$W = \int_0^H \int_L^{2L} \left[\frac{1}{2}|\nabla A|^2 - 4\pi p_{\text{int}}(z)\beta_0^{-1}F(A)\right] dx\,dz. \qquad (6)$$

The minimization is done by varying the A-values on a grid of 120×240 cells, using the conjugate-gradient method (Press et al. 1992). A similar technique was used in Hasan et al. (2003), where we constructed a model of a very thin flux tube (see the Appendix of that paper), and in Cranmer & van Ballegooijen
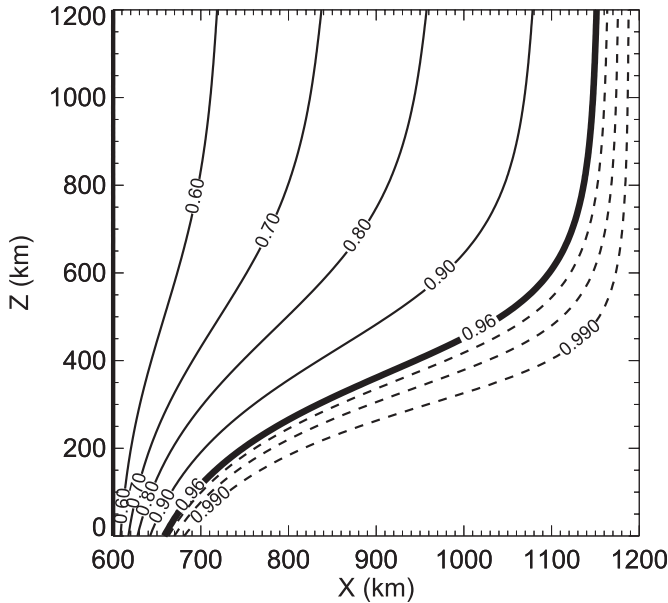
FIG. 2.—Magnetic field lines (*solid curves*) in the right half of a flux tube. Each line is annotated by the fractional flux $f = A/A_{max}$ with respect to the left boundary $x = 0$. The heavy solid line representing $f = 0.96$ has been chosen to represent the interface of the tube with the ambient medium (with weak field). The dashed curves denote field lines at $f = 0.97, 0.98$, and 0.99.

TABLE 1
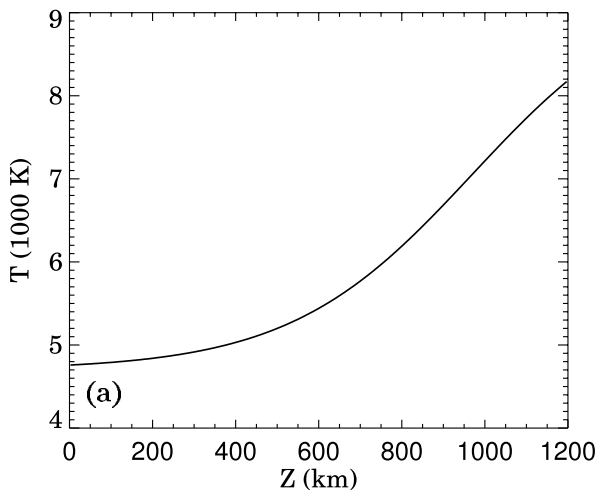PARAMETERS ON THE TUBE AXIS AND AMBIENT MEDIUM

VARIABLE	TUBE AXIS		AMBIENT MEDIUM	
	Base	Top	Base	Top
Temperature (K)	4800	8200	4800	8200
Density (g cm^{-3})	1.3×10^{-7}	9.5×10^{-12}	4.0×10^{-7}	2.9×10^{-11}
Pressure (dyn cm^{-2})	4.1×10^{4}	8.2	1.2×10^{5}	22
Sound speed (km s^{-1}).....	7.1	12	7.1	12
Alfvén speed (km s^{-1})....	11	92	0.30	52
Magnetic field (G)	1400	100	70	100
β	0.5	0.02	600	0.06

layers) across which the field drops rapidly to a small value. We refer to this weak field region as the external or ambient medium. There is, however, a smooth transition of gas pressure from the interior to the exterior of the sheet.

The internal pressure as a function of height was approximated as a sum of two exponentials:

$$p_{int}(z) = p_1 \exp(-z/H_1) + p_2 \exp(-z/H_2), \qquad (8)$$

with a photospheric pressure scale height of $H_1 = 110$ km and a chromospheric scale height of $H_2 = 220$ km. To obtain kilogauss fields in the photosphere, we used $\beta_0 = 0.5$, so that the external gas pressure is 3 times the internal gas pressure.

In the present calculations we consider a full flux sheet placed symmetrically with respect to the midpoint of the computational domain ($x = L$), which we take to be a square of size 1200 km with a uniform grid of 240×240 cells, corresponding to a mesh spacing of 5 km in either direction. We take $L = 600$ km so that the flux tube axis is at $x = 600$ km and redefine A_{max} to be the total magnetic flux in the flux sheet [$A(L, 0) = 0.5A_{max}$].

Figure 2 depicts the magnetic field lines in the equilibrium state in the right half of the flux tube. Each field line is annotated by the fractional flux $f \equiv A/A_{max}$ as measured from the left edge of the computational domain. Thus, $f = 0.5$ corresponds to the tube axis at $x = 600$ km. The heavy solid line corresponding to $f = 0.96$ has been arbitrarily chosen to denote the field line demarcating the interface between the tube and the ambient medium (with weak field). In practice, the precise choice of f for the boundary line does not matter as long as $f \approx 1$ at the interface.
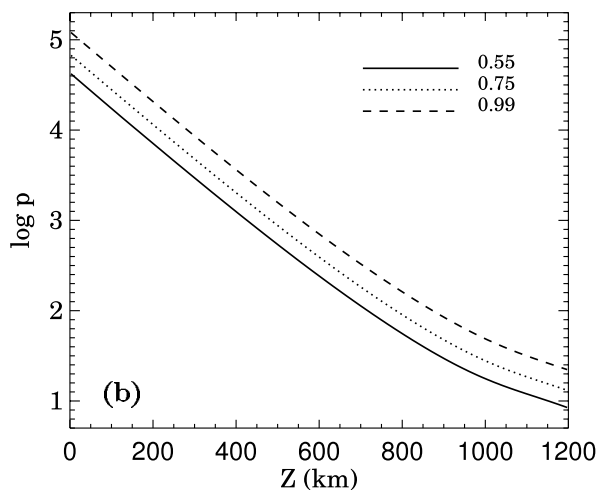
(2005). In these papers a Lagrangian description was used, and the radial positions $r(\Phi, z)$ varied on a fixed grid of Φ (the flux function in cylindrical coordinates) and height z. In the present paper we vary $A(x, z)$ on a fixed grid of x and z.

A model containing one whole flux sheet can be obtained by mirroring the field with respect to $x = L$, and models containing multiple sheets can be obtained by further mirroring with respect to $x = 2L$. The resulting fields will be used as initial conditions for the two-dimensional MHD calculation (see § 3).

We perform calculations for a single sheet using the following form for $F(A)$:

$$F(A) = \frac{4}{3}\left(\frac{A}{A_{max}}\right)^2 - \frac{1}{3}\left(\frac{A}{A_{max}}\right)^8 \quad \text{if } A \le A_{max}. \qquad (7)$$

The resultant field configuration in the flux sheet, as we see below, has a sharp interface (especially in the photospheric

FIG. 3.—Variation of (*a*) the temperature T and (*b*) the logarithm of the pressure p as a function of height on the field lines corresponding to $f = 0.55$ (*solid curve*), 0.75 (*dotted curve*), and 0.99 (*dashed curve*) in the equilibrium configuration. Note that the temperature is uniform (by assumption) in the horizontal direction.
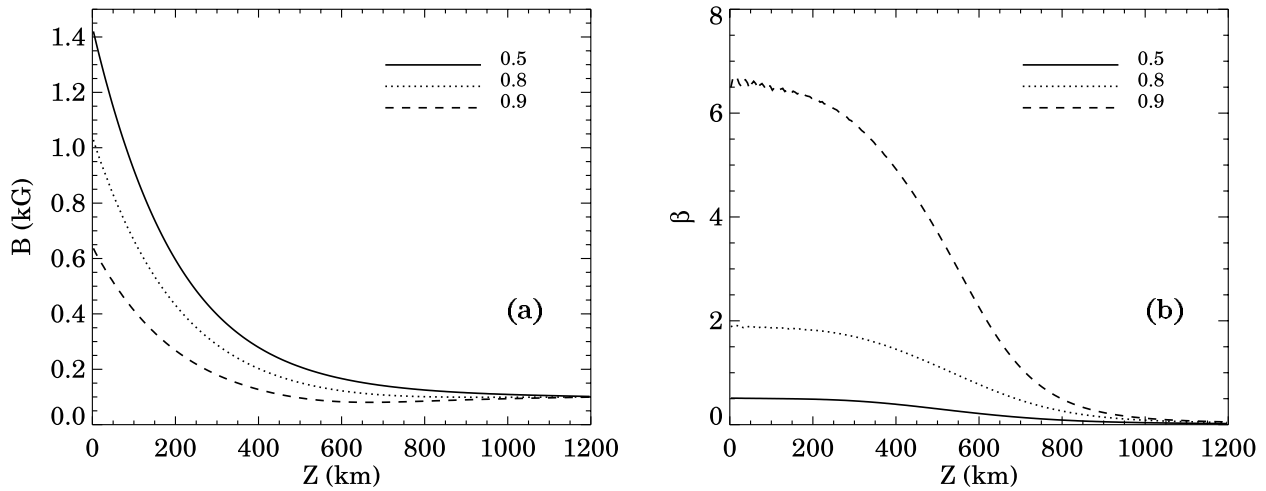
Fig. 4.—Variation of (*a*) the magnetic field strength *B* and (*b*) β as a function of height on the field lines corresponding to *f* = 0.5 (*solid curve*), 0.8 (*dotted curve*), and 0.9 (*dashed curve*) in the equilibrium configuration.

To illustrate this, we also show field lines (*dashes*) corresponding to $f = 0.97$, 0.98, and 0.99. Close to the lower boundary, the separation between these lines is insignificant (at $z = 0$ the distance between them for $f = 0.96$ and 0.99 is about 20 km). Above $z = 400$ km, most of the region is filled with field lines and so effectively there is no external medium above these layers. There is, however, a small height range below $z = 400$ km where the position of the interface depends on the *f* value chosen for the interface. But at these heights the field is rather weak ($\beta > 50$). The essential point is that close to the lower boundary (where wave excitation occurs) the magnetic flux is confined to a well-defined region with a width of about 150 km containing 99% of the magnetic flux.

Table 1 provides some of the parameters of the equilibrium model on the tube axis and in the ambient medium (taken at $f = 0.99$) at the base ($z = 0$) and the top ($z = 1200$ km) of the computational domain. The sound speed c_S varies from 7.1 km s^{-1} at $z = 0$ to 9.2 km s^{-1} at $z = 1200$ km. The ambient medium is, as stated before, not field-free. At the base of the tube, the field drops rapidly outside the interface and this region is effectively field-free in view of the large value of β.

Figures 3*a* and 3*b* depict the variation with height of the temperature and pressure, respectively. It should be noted that the temperature by assumption is constant in the horizontal direction. In Figure 3*b*, the pressure is shown on different field lines. The dashed curve ($f = 0.99$) essentially depicts the height variation of the pressure in the weak field medium where $\beta \gg 1$.

Figures 4*a* and 4*b* show the height variation of the magnetic field strength *B* and of β on various field lines, parameterized by $f = 0.5$, 0.8, and 0.9. The field strength on each of the field lines drops rapidly with *z* in the first few hundred kilometers, after which it approaches a constant value of about 100 G. On the other hand, β is practically constant with *z* in the lower region of the atmosphere, which is similar to the behavior one finds in a thin flux tube with equal internal and external temperature at the same height (e.g., see Hasan et al. 2003), and where both B^2 and *p* have the same height dependence. In the upper part of the flux tube, *B* is constant and β drops off sharply with *z*, essentially mimicking the *p* dependence. The Alfvén speed, which is related to β by the approximate relation $v_A \approx c_S/\sqrt{\beta}$, is almost constant (with height) in the lower regions of the atmosphere in the tube, but increases sharply with *z* in the higher layers.
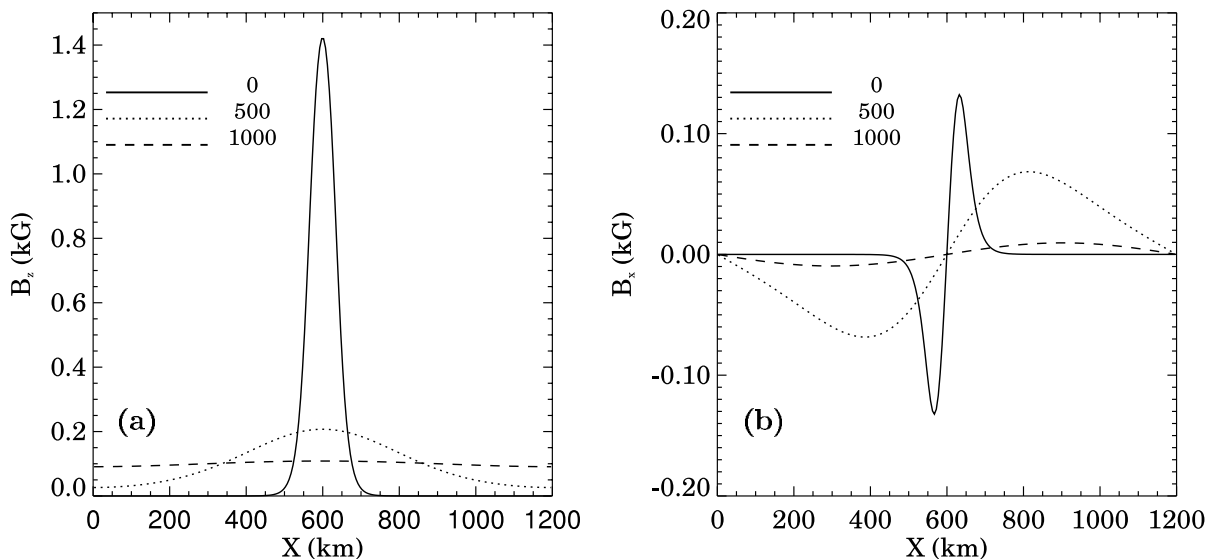

Fig. 5.—Variation of (*a*) B_z and (*b*) B_x with horizontal distance (from the left edge of the computational domain) at the following heights: $z = 0$ (*solid line*), 500 km (*dotted line*), and 1000 km (*dashed line*).

Figure 5 shows the variation with horizontal distance x of (a) the vertical component of the magnetic field B_z and (b) the horizontal component B_x at various heights, $z = 0$ (*solid line*), 500 (*dotted line*), and 1000 km (*dashed line*). The solid lines clearly show that the magnetic field at the base is confined to a width of about 150 km. At a height of 1000 km, B_x becomes very small (a few gauss) and the field is essentially vertical and constant (approximately 100 G) in the horizontal direction.

3. METHOD AND BOUNDARY CONDITIONS

We consider wave generation in the configuration described in the previous section by perturbing the lower boundary and solving the two-dimensional magnetohydrodynamic (MHD) equations in conservation form for an inviscid adiabatic fluid. These consist of the usual continuity, momentum, entropy (without sources), and magnetic induction equations (for details see Steiner et al. 1994). The unknown variables are the density, momentum, entropy per unit mass, and magnetic field. We assume that the plasma consists of fully ionized hydrogen with a mean molecular weight of 1.297. The temperature is computed from the specific entropy, and the pressure is found using the ideal gas law.

The above MHD equations are solved following the numerical procedure given by Steiner et al. (1994). Briefly, the equations are discretized on a two-dimensional mesh using a finite-volume method, which has the advantage of preserving $\nabla \cdot \boldsymbol{B} = 0$ to machine accuracy. The method employs finite differences to compute numerical fluxes based on the flux-corrected transport (FCT) scheme of Oran & Boris (1987). The time integration is explicit and has second-order accuracy in the time step. Small time steps are required to satisfy the Courant condition in the upper part of the domain, where the Alfvén speed is large.

Periodic boundary conditions are used at the horizontal boundaries. At the top boundary, (1) the vertical and horizontal components of momentum are set to zero; (2) the density is determined using linear logarithmic extrapolation; (3) the horizontal component of the magnetic field and temperature are set equal to the corresponding values at the preceding interior point. The vertical component of the magnetic field is determined using the condition $\nabla \cdot \boldsymbol{B} = 0$. Similar conditions are used at the lower boundary, except for the density, temperature and horizontal component of the velocity (or momentum). The density is obtained using cubic spline extrapolation, the temperature is kept constant at its initial value and v_x at $z = 0$ is specified as follows:

$$v_x(x, \ 0, \ t) = v_0 \sin (2\pi t/P), \qquad (9)$$

where v_0 denotes the amplitude of the horizontal motion and P is the wave period. This form was chosen to simulate the effect of transverse motion of the lower boundary. For simplicity, we assume that all points at the lower boundary have this motion, since this does not generate any waves in the ambient medium, other than at the interface with the flux tube, as we see below.

4. DYNAMICS OF A FLUX SHEET

In § 2, we presented a model for a single flux sheet in static equilibrium. The stability of this equilibrium was checked by solving the time-dependent two-dimensional MHD equations without any external driving (assuming rigid boundaries in the vertical direction). We found that this equilibrium was maintained to high accuracy. The maximum amplitude of the flows was no more than a few meters per second over timescales greater than the sound travel time (in both the vertical and horizontal directions), corresponding to over 10,000 time steps.

Let us now consider wave generation in the equilibrium atmosphere by means of a transverse motion at the lower boundary ($z = 0$) of the atmosphere, which displaces the flux sheet. We focus on two limiting cases, corresponding to impulsive and periodic excitation, respectively.

4.1. *Impulsive Excitation*

This case corresponds to uniform displacement of the lower boundary at $z = 0$ to the right, which lasts half a wave period ($P = 240$ s) and then stops. The peak transverse velocity is $v_0 = 750$ m s^{-1}. Figures 6a–6d show, at times of 52, 82, 109, and 136 s, respectively, the velocity field (*arrows*), the magnetic field (*black lines*) and the temperature change $\Delta T = T - T_0$, where T_0 is the initial temperature at each height. The maximum value of the velocity and the color table for the temperature are shown on the right of each figure. We have omitted velocities smaller than 30 m s^{-1}. The white lines denote contours of constant β for values of $\beta = 0.1, 0.5, 1.0$ (*thick line*), and 10.

The horizontal motion of the flux tube at the lower boundary pushes the field lines uniformly to the right. In the flux tube, this motion is communicated to the upper layers as a fast mode, which travels with the local Alfvén speed. The transverse motion of the field lines compresses the gas on the right interface of the tube and the ambient medium (above the base, where there is no horizontal motion in the field-free medium).

Figure 7 clearly shows at $t = 82$ s the development of a pressure enhancement and depletion, respectively, at the right and left interfaces of the tube with respect to the field-free gas. This essentially creates a pressure dipole that in turn generates a vortex motion with upflow and downflow motions on the right and left sides, respectively. The top of the vortex motion is in the opposite direction to that at the base. From Figure 6 we find that as time proceeds, the vortex grows in size and also moves upward. This motion carries the field lines, pushing them slightly counterclockwise in the lower regions of atmosphere.

As the vortex extends upward, there is a hint of a shock forming at its upper edge, as can be seen in Figure 6c. Once the transverse driving motion stops at the base, the vortex motions diminish and the flow is now guided along the field lines. This is evident in Figure 6d, which shows at $t = 136$ s negligible flows near the base of the flux tube and large flows almost aligned with the magnetic field in the upper atmosphere. The large upflows generate a shock that can be discerned at a height of about 900 km along with a temperature enhancement greater than 400 K.

Figures 8a and 8b denote the z-variation of v_s and v_n, the field-aligned and normal velocity components respectively at 82, 109, and 150 s along a specific field line. We choose a field line parameterized by $f = 0.6$, which is just to the right of the flux tube axis. Let us first consider the behavior of the field-aligned flow, shown in Figure 8a. As time proceeds, the vertical component of the velocity pulse increases with height in magnitude on account of the density stratification and it steepens on account of nonlinear effects as it propagates upward. At $t = 150$ s the pulse resembles a shock. The presence of a wake behind the shock should also be noted, which is a generic feature associated with the propagation of a pulse in a vertically stratified atmosphere (e.g., Hasan et al. 2003). Figure 8b shows the z-variation of the normal component of the flow. The curves corresponding to $t = 82$ and 109 s show the normal component profiles during the impulsive phase (i.e., during the time interval that transverse driving motions are present at $z = 0$). The dashed curve shows the profile at $t = 150$ s, after the transverse motion at the base has halted. This profile is broadened due to
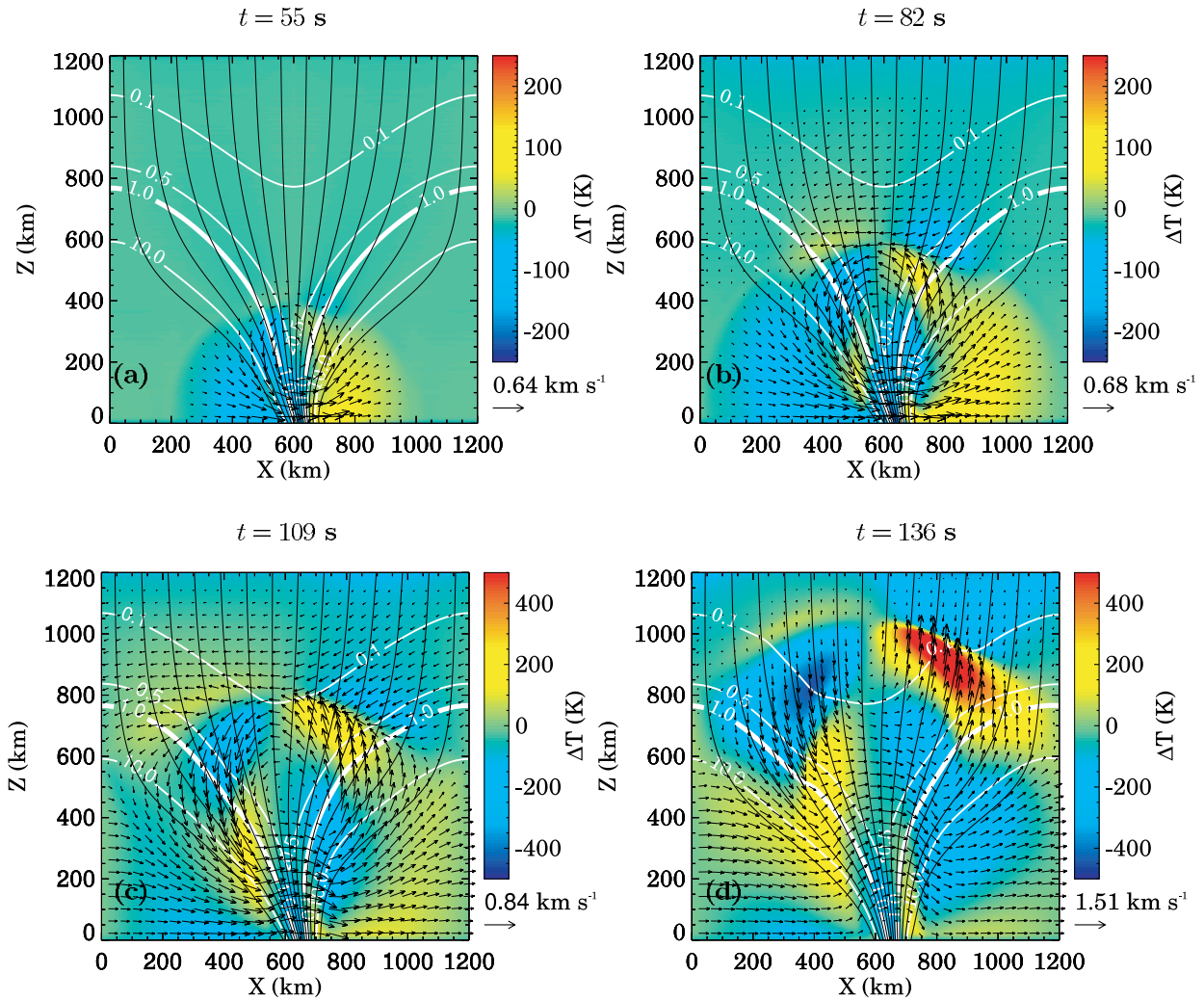
FIG. 6.—Flow pattern and temperature perturbation, ΔT (about the initial state), at (a) 55 s, (b) 82 s, (c) 109 s, and (d) 136 s in a network element due to horizontal motion at the lower boundary, with an amplitude of 750 m s^{-1}, applied for half a wave period ($P = 240$ s), after which the motion ceases. The thin black curves are the magnetic field lines, the arrows denote the direction of the flow, and the color scale shows the temperature perturbation. The white curves denote contours of constant β corresponding to $\beta = 0.1$, 0.5, 1.0 (thick curve), and 10.

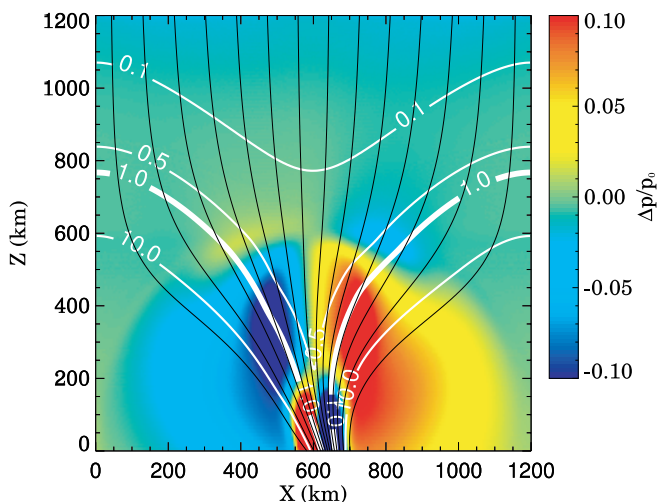

FIG. 7.—Relative pressure perturbation (about the initial state), $\Delta p/p_0$, at $t = 82$ s in a network element due to horizontal motion at the lower boundary with an amplitude of 750 m s^{-1} and a period of $P = 240$ s. The thin black curves are the magnetic field lines, and the white curves denote contours of constant β corresponding to $\beta = 0.1$, 0.5, 1.0 (thick curve), and 10.

the fact that the Alfvén speed, which is the characteristic propagation speed of the transverse pulse, increases sharply with height. In the lower regions of the atmosphere, where $\beta \approx 0.6$, $v_A \approx 10$ km s^{-1}, whereas at a height of 600 km, it has increased to about 18 km s^{-1}.

4.2. Periodic Excitation

We now consider the periodic excitation of waves due to transverse driving of the lower boundary, with a period of 24 s (similar to Rosenthal et al. [2002] and Bogdan et al. [2003]), although with a higher amplitude of 750 m s^{-1}. Figures 9a–9d show the wave pattern that develops in this case. As before, the colors are used to denote the temperature perturbation with respect to the initial value at each height and the white curves depict contours of constant β.

The horizontal motion of the tube at the lower boundary is a source of acoustic waves at the interface. These waves propagate isotropically in the ambient medium and near the interface (or more precisely in the region where $\beta \gg 1$) as "spherical" acoustic waves. The yellow and blue strips associated with ΔT, with an almost constant separation, clearly show the acoustic waves propagating outward at the sound speed from their source near the bottom edge of the tube. The wavelength of these waves
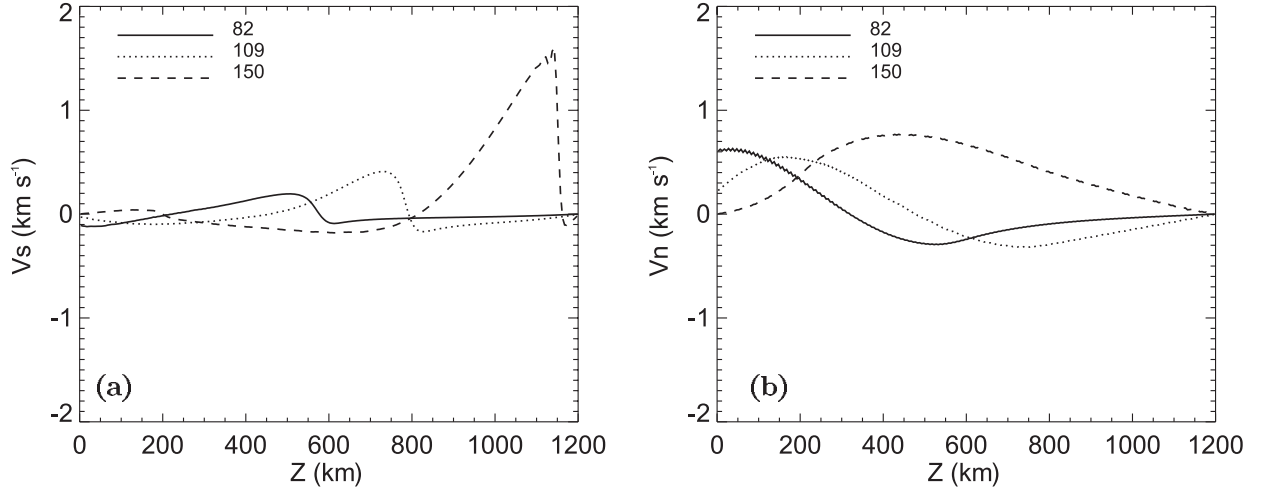
FIG. 8.—Variation of the velocity components (*a*) along the magnetic field v_s and (*b*) normal to the magnetic field v_n at $t = 82$ s (*solid curve*), 109 s (*dotted curve*), and 150 s (*dashed curve*) on a field line characterized by $f = 0.6$ in a network element due to a horizontal motion at the lower boundary with an amplitude of 750 m s^{-1} and a period $P = 240$ s.
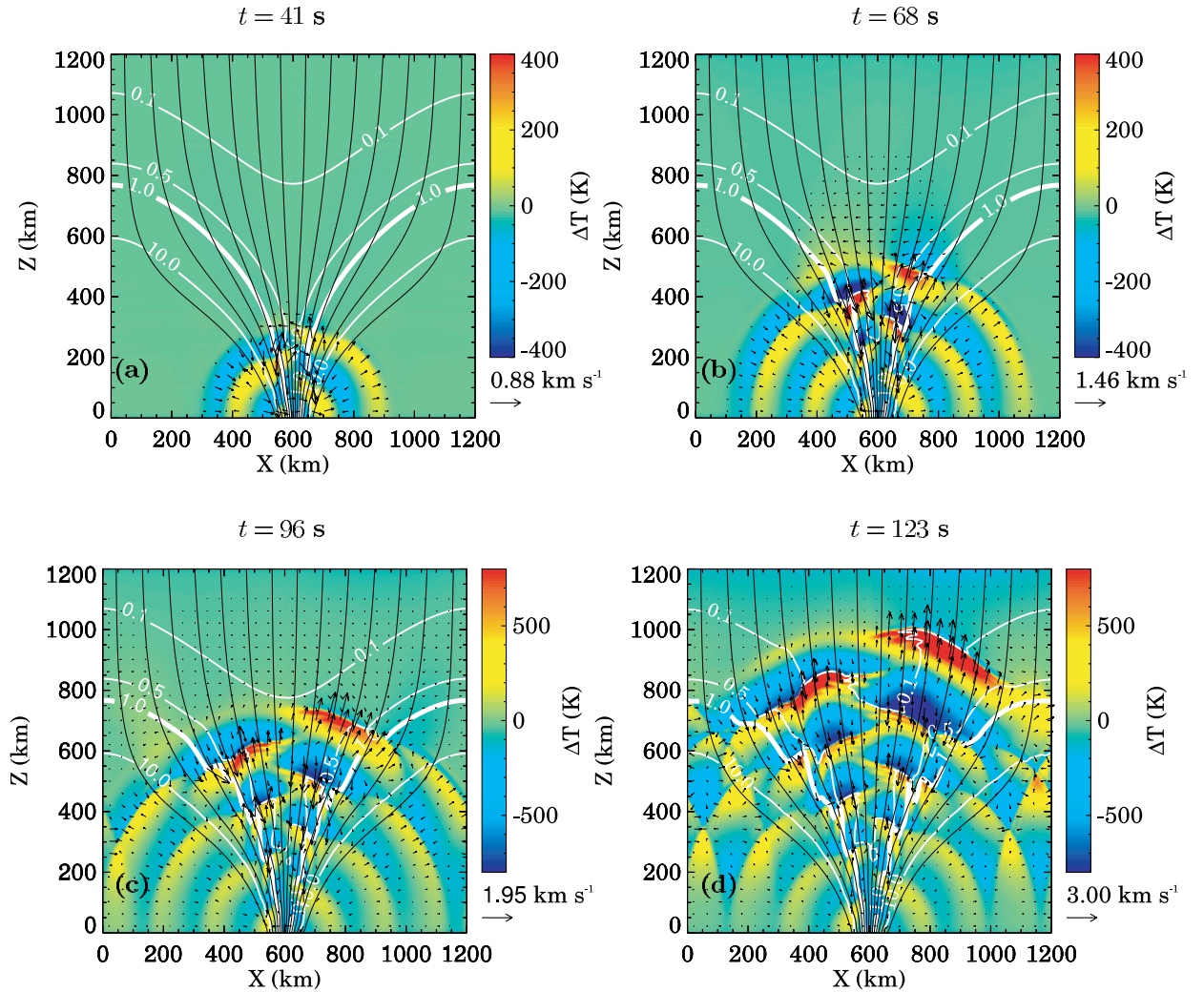

FIG. 9.—Flow pattern (*arrows*) and the temperature perturbation (about the initial state), ΔT, at (*a*) 41 s, (*b*) 68 s, (*c*) 96 s, and (*d*) 123 s in a network element due to a periodic horizontal motion at the lower boundary with an amplitude of 750 m s^{-1} and a wave period of $P = 24$ s. The thin black curves represent the magnetic field lines. The white curves denote contours of constant β corresponding to $\beta = 0.1$, 0.5, 1.0 (*thick curve*), and 10.
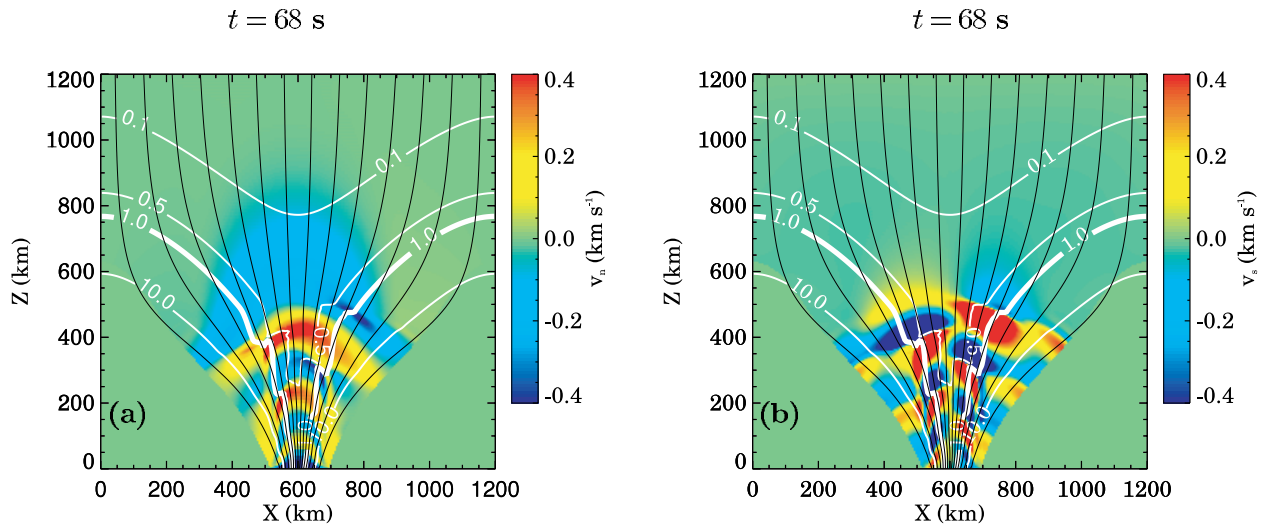
Fig. 10.—Velocity components (*a*) v_n, normal to the field, and (*b*) v_s, along the field, at $t = 68$ s in a network element due to a horizontal motion at the lower boundary with an amplitude of 750 m s^{-1} and a period of $P = 24$ s. The thin black curves represent the magnetic field lines, and the white curves denote contours of constant β, corresponding to $\beta = 0.1$, 0.5, 1.0 (*thick curve*), and 10.

is approximately constant, since the acoustic speed varies weakly in the lower part of the computational domain.

In the flux tube, the horizontal driving motions generate both fast and slow modes. Close to the tube axis, the field is strong ($\beta < 1$) and the transverse motion generates a fast wave that propagates upward at the Alfvén speed. Its propagation can be clearly seen in Figure 10*a*, which depicts at $t = 68$ s the variation of the normal velocity component v_n as a color contour plot. The fast wave front shows an asymmetry in propagation, since the Alfvén speed is largest on the tube axis and decreases in the horizontal direction. On the axis the Alfvén speed is 10 km s^{-1} at $z = 0$, 18 km s^{-1} at $z = 600$ km, and 30 km s^{-1} at $z = 800$ km (the last is roughly the height at which the fast mode has reached as can be seen from the blue halo). The increase in separation in the vertical direction between the color peaks clearly shows the increase in wavelength due to the increase in Alfvén speed with z.

The horizontal motions at the lower boundary produce compressions and decompressions of the gas in the tube, where

$\beta \gtrsim 1$. The resulting pressure variations are periodic in height and time and are $180°$ out of phase on opposite sides of the tube axis, as can be seen in Figure 11, which depicts the relative pressure perturbation in the network element. The associated pressure gradients drive periodic vertical flows that propagate upward along the field lines of the flux tube at approximately the acoustic speed. These motions can be discerned in Figure 10*b*, which shows at $t = 68$ s the velocity component along the field. The vertical flows are an integral part of the flux tube wave, so the wave has both transverse and longitudinal character in different parts of the tube.

As a wave emanating from the lower boundary, where $\beta > 1$, travels upward along field lines, it reaches layers where $\beta = 1$. In such regions, the wave changes character and undergoes mode conversion, which has been discussed in some detail by Rosenthal et al. (2002) and Bogdan et al. (2003). In the low-β region, the wave consists of two almost decoupled parts: a fast
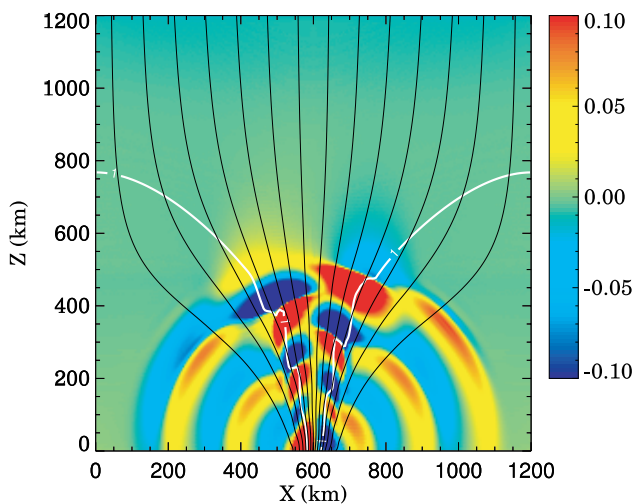

Fig. 11.—Relative pressure perturbation (about the initial state), $\Delta p/p_0$, at $t = 68$ s in a network element due to horizontal motion at the lower boundary with an amplitude of 750 m s^{-1} and a period of $P = 24$ s. The thin black curves represent the magnetic field lines, and the white curve denotes the contour $\beta = 1$.
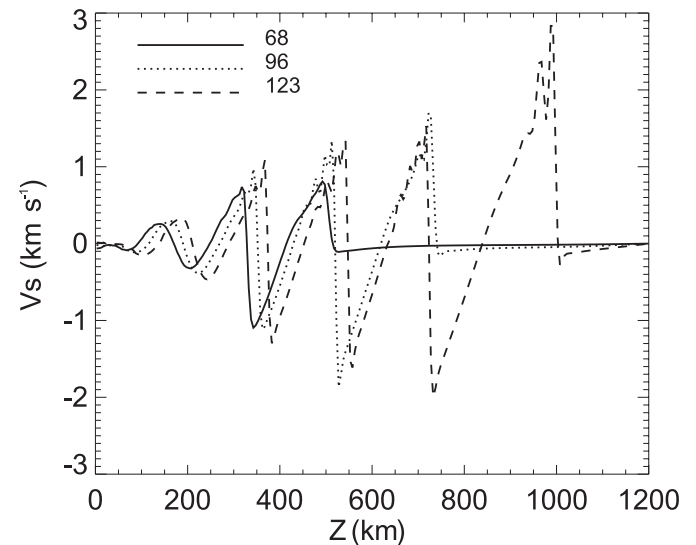

Fig. 12.—Variation of the velocity component along the magnetic field, v_s, at times $t = 68$ s (*solid curve*), 96 s (*dotted curve*), and 123 s (*dashed curve*) on a field line characterized by $f = 0.6$ in a network element due to horizontal motion at the lower boundary with an amplitude of 750 m s^{-1} and a period of $P = 24$ s.

mode, described in the preceding paragraph (see Fig. 10a), and a slow mode that is guided along the field lines. The slow modes on opposite sides of tube axis as stated earlier are $180°$ out of phase with each other, and their amplitudes increase with height due to the density stratification. Being mainly acoustic in nature, they produce a compression and heating of the plasma in the chromosphere. This can be seen for instance in Figure 9d, where the wave front located at a height of about 1000 km produces heating greater than 500 K. Figure 12 shows the variation of the field-aligned velocity component, v_s, on a field line $f = 0.6$ at three different times, shown by the different curves. One can see the amplitude increase and steepening of the wave due to nonlinear effects as it propagates upward at the acoustic speed of around 7 km s^{-1}. This clearly establishes the nature of this wave as acoustic. It is interesting to note the occurrence of weak shocks at a Mach number of about 0.2.

5. DISCUSSION AND SUMMARY

The present investigation is a continuation of our earlier work on the dynamics of the magnetic network on the Sun. In our previous studies we used a simplified picture of magnetic elements in terms of a quasi one-dimensional treatment based on the thin flux tube approximation. This approach was useful in providing a qualitative picture of wave propagation and nonlinear mode coupling in the lower regions of the atmosphere where the thin flux tube approximation is applicable. However, as already pointed out in § 1, this approximation breaks down in the chromosphere due to the expansion of the flux tube with height as well as due to the merging of different tubes. We overcome these limitations by using a two-dimensional treatment. In the first part of this study we focus on a single flux tube and examine the consequences when the lower boundary is perturbed by a transverse motion. Future work will extend the present analysis to multiple tubes as well as other types of excitation mechanisms.

The choice of using a transverse velocity perturbation at the lower boundary was to some extent motivated by observations, particularly those of Muller & Roudier (1992) and Muller et al. (1994), who studied the footpoint motions of a large number of network bright points, generally regarded as a proxy for magnetic elements. We considered the driving motions to occur at a fixed height in the atmosphere. In reality, we expect that the displacement of the flux tubes occurs in response to turbulent motions below the photospheric base. These flows are absent or weak on the surface. Thus, the pressure fluctuations in our model are a direct consequence of the relative motion of the flux tube with respect to its local surroundings. These play a key role in driving the vortex motions that propagate high up in the flux tube. It appears reasonable to expect that such pressure fluctuations indeed occur in the solar network.

We chose two limiting forms for the time behavior of the perturbation as an idealization for drivers that (1) generate discrete pulses well separated in time and (2) are periodic and continuous. The values of the time constant for the pulse in the first case and the wave period in the second case were chosen because of practical considerations related to the limit of not letting the simulation exceed a total time at which reflections from the top boundary become important.

We find that the transverse driving motions at the lower boundary lead to strong pressure perturbations in the field-free medium at the tube interface. This is an efficient process for generating vortical motions, recognized earlier by Shibata (1983) in two-dimensional simulations, who found that such motions can arise due to a pressure perturbation applied at the base of a uniformly magnetized stratified atmosphere ($\beta > 1$). In our simulations the strong pressure fluctuations are essentially localized in regions where β is greater than unity. The observational signature associated with vortex formation would be the prediction of simultaneous upward and downward motions on opposite sides of flux tubes. Under what conditions does a vortex form? It appears that for wave periods that are sufficiently long (compared to the Alfvén travel time) the dynamics is likely to be dominated by vortical motions, but it is difficult at this stage to say anything more definitive.

An important consequence of our calculations is that the interface between the flux tube and the ambient medium is both a source of acoustic waves in the ambient medium as well as fast and slow waves inside the flux tube. This can have interesting consequences: the acoustic waves that travel isotropically in the field-free medium will impinge on neighboring flux tubes in the network and excite waves in them. On the other hand, the modes generated in the high-β region of the tube (at the interface) undergo mode conversion as they propagate upward and enter layers in the atmosphere where $\beta \approx 1$, as also found by Rosenthal et al. (2002) and Bogdan et al. (2003). In the upper part of the flux tube, where the field is essentially vertical and $\beta \ll 1$, the acoustic-like longitudinal motions steepen and form shocks accompanied by heating, as also found out for instance by Hasan & Ulmschneider (2004) using a thin flux tube calculation. There is, however, an important qualitative difference between the present results and those of Zhugzhda et al. 1995, Hasan et al. (2003), and Hasan & Ulmschneider (2004). In the latter, longitudinal motions are generated from transverse driving motions at the flux tube footpoints as a consequence of nonlinear mode coupling that is most efficient when the transverse and longitudinal mode speeds are comparable (roughly for $\beta \approx 0.2$). In the present work, the mode conversion occurs essentially in the linear regime and is a consequence of the spatial variation of β in the tube. We find that transverse driving motions with velocities less than 1 km s^{-1} are sufficient to produce strong shocks in the chromosphere.

The present work is in the spirit of the investigations by Rosenthal et al. (2002) and Bogdan et al. (2003) on wave propagation in two-dimensional magnetic structures. There are, however, qualitative differences between the initial state and the form of the perturbation used for driving the atmosphere in the two sets of calculations. For instance, the initial equilibrium configuration adopted by the above authors assumes a potential field that is typical of the large-scale pattern connecting different network regions. Bogdan et al. (2003) consider a unipolar magnetic structure that at the base is 2000 km wide surrounded by smaller magnetized regions (about 750 km wide) of opposite polarity (as shown in Fig. 1 of their paper). At larger horizontal distance from the flux concentration, the field is essentially horizontal although much weaker. Thus, in the above configuration the entire atmosphere is magnetized. On the other hand, we consider a nonpotential unipolar magnetic element representative of a tube in a network element that is initially in magnetostatic equilibrium and in which the flux at the photospheric level is effectively confined inside a tube with a transverse dimension of about 150 km. In such a model β is much higher in the ambient medium than in a corresponding potential model although in the central regions of the tube the field strengths are comparable. The essential difference, though, is in the sharp decline of the field strength across the interface in our nonpotential model. It is possible that this difference may not be crucial for wave propagation, which is most likely influenced by the field in the central region of the tube up to the curve corresponding to $\beta \approx 1$. In the tube and ambient medium where $\beta \gg 1$, the acoustic (or more precisely the acoustic-gravity) waves are insensitive to the precise value of β, as long

as it is sufficiently large (we are grateful to the referee for drawing our attention to this fact).

However, we believe that the relatively well defined sharp interface between the flux tube and ambient medium in our model is responsible for the efficient acoustic wave emission at the tube edge. This is because such waves can be strongly excited in the narrow layer between the rigid interface of the flux tube and ambient medium against which the former is pressed. If the boundary is smooth, this region is wider and suffers less compression. On the other hand, if the boundary is sharp and discontinuous, with the interior field strong everywhere, this transition layer would not exist and the wave emission at the edge would again be weak. We hope to pursue this line of investigation in future work.

In our model the whole flux tube at the photosphere is displaced and not just a small region inside it. The driving motion in the simulations of Bogdan et al. (2003) is confined to a region about 400 km wide within the flux element. In our simulations, the transverse motion of the entire magnetic element creates strong pressure perturbations just outside the tube that in turn are responsible for the vortical motions and the generation of acoustic waves in the ambient medium as well as the strong longitudinal motions that eventually produce shock heating in the upper atmosphere. The fact that the flux tube interface is a source of acoustic waves in the ambient medium is a new feature of the present work that does not appear to have received adequate attention and as stated earlier would probably not be noticeable in a distributed field configuration such as corresponding to a potential field.

A further difference between our model and that of Bogdan et al. (2003) is that we consider impulsive excitation in addition to periodic excitation. We also consider a nonisothermal atmosphere with the temperature increasing with height that is representative of the solar chromosphere.

We should point out some limitations of our current study. Our analysis is based on a two-dimensional treatment in slab geometry, assuming that fluid displacements are confined to the x-z plane. The waves examined by us are different from the kink and sausage modes treated earlier by us using a simplified thin flux tube approximation. Ideally, one would use a three-dimensional treatment, which is currently beyond the scope of this work. Our analysis also neglects the torsional Alfvén wave, which in reality would couple to the fast and slow modes. Even within the two-dimensional framework, we have had to restrict the height range in our simulations to 1200 km, since the Alfvén speed (that essentially controls the time step used in the numerical scheme) increases very rapidly with z.

In summary, this paper is the first of a series of investigations on the dynamics of the solar magnetic network based on a two-dimensional treatment of the MHD equations. We have made a start by considering processes occurring in a single flux tube that expands with height in the photosphere and assumes a "wine glass" geometry in the chromosphere. Flows and wave motions are generated in this configuration by transverse motions at the base of the flux tube. For impulsive driving we find the presence of vortical motions. An interesting feature for both impulsive and periodic driving is the development of shock-like features in the upper atmosphere, which can be important in heating the chromosphere. We hope to extend the scope of the present calculation in future work to include multiple flux tubes as well as include a larger height extension in order to estimate transport of energy in to the corona through this mechanism.

REFERENCES

Bogdan, T. J., et al. 2003, ApJ, 599, 626
Cargill, P. J., Spicer, D. S., & Zalesak, S. T. 1997, ApJ, 488, 854
Carlsson, M., & Stein, R. F. 1995, ApJ, 440, L29
Choudhuri, A. R., Auffret, H., & Priest, E. R. 1993, Sol. Phys., 143, 49
Cranmer, S. R., & van Ballegooijen, A. A. 2005, ApJS, 156, 265
Curdt, W., & Heinzel, P. 1998, ApJ, 503, L95
Fawzy, D., Rammacher, W., Ulmschneider, P., Musielak, Z. E., & Stępień, K. 2002, A&A, 386, 971
Grossmann-Doerth, U., Kneer, F., & von Uexküll, M. 1974, Sol. Phys., 37, 85
Hasan, S. S., & Kalkofen, W. 1999, ApJ, 519, 899
Hasan, S. S., Kalkofen, W., & van Ballegooijen, A. A. 2000, ApJ, 535, L67
Hasan, S. S., Kalkofen, W., van Ballegooijen, A. A., & Ulmschneider, P. 2003, ApJ, 585, 1138
Hasan, S. S., & Ulmschneider, P. 2004, A&A, 422, 1085
Hollweg, J. V., Jackson, S., & Galloway, D. 1982, Sol. Phys., 75, 35
Huang, P., Musielak, Z. E., & Ulmschneider, P. 1995, A&A, 297, 579
Kalkofen, W. 1997, ApJ, 486, L145
Lites, B. W., Rutten, R. J., & Kalkofen, W. 1993, ApJ, 414, 345
McAteer, R. T. J., Gallagher, P. T., Williams, D. R., Mathioudakis, M., Bloomfield, D. S., Phillips, K. J. H., Keenan, F. P. 2003, ApJ, 587, 806
McAteer, R. T. J., Gallagher, P. T., Williams, D. R., Mathioudakis, M., Phillips, K. J. H., & Keenan, F. P. 2002, ApJ, 567, L165
Muller, R., & Roudier, Th. 1992, Sol. Phys., 141, 27

Muller, R., Roudier, Th., Vigneau, J., & Auffret, H. 1994, A&A, 283, 232
Noble, M. W., Musielak, Z. E., & Ulmschneider, P. 2003, A&A, 409, 1085
Ofman, L., & Davila, J. M. 1998, J. Geophys. Res., 103, 23677
Ofman, L., Nakariakov, V. M., & DeForest, C. E. 1999, ApJ, 514, 441
Oran, E. S., & Boris, J. P. 1987, Numerical Simulations of Reactive Flow (New York: Elsevier)
Press, W. H., Teukolsky, S. A., Vetterling, W. T., & Flannery, B. 1992, Numerical Recipes in FORTRAN (2nd ed.; Cambridge: Cambridge Univ. Press)
Rosenthal, C. S., et al. 2002, ApJ, 564, 508
Rutten, R. J., & Uitenbroek, H. 1991, Sol. Phys., 134, 15
Sakai, J. I., Igarashi, J., & Kawata, T. 1998, Sol. Phys., 181, 13
Shibata, K. 1983, PASJ, 35, 263
Skumanich, A., Smythe, C., & Frazier, E. N. 1975, ApJ, 200, 747
Spruit, H. C. 1981, A&A, 102, 129
Steiner, O., Knölker, M., & Schüssler, M. 1994, in Solar Surface Magnetism, ed. R. J. Rutten & C. J. Schrijver (NATO ASI Ser. C-433; Dordrecht: Kluwer), 441
Ulmschneider, P. 2003, in Lectures on Solar Physics, ed. H. M. Antia, A. Bhatnagar, & P. Ulmschneider (Heidelberg: Springer) 232
Ulmschneider, P., Zähringer, K., & Musielak, Z. E. 1991, A&A, 241, 625
von Uexküll, M., & Kneer, F. 1995, A&A, 294, 252
Zhugzhda, Y. D., Bromm, V., & Ulmschneider, P. 1995, A&A, 300, 302